Inorganic Chemistry

ARTICLE

pubs.acs.org/IC

Ratiometric Fluorescent Sensor Based on Inhibition of Resonance for Detection of Cadmium in Aqueous Solution and Living Cells

Lin Xue,[†] Guoping Li,[†,‡] Qing Liu,[†,‡] Huanhuan Wang,[†,‡] Chun Liu,[§] Xunlei Ding,[†] Shenggui He,[*,†] and Hua Jiang[*,†]

[†]Beijing National Laboratory for Molecular Sciences, Institute of Chemistry, Chinese Academy of Sciences, Beijing 100190, People's Republic of China

[§]State Key Laboratory of Fine Chemicals, Department of Chemical Engineering, Dalian University of Technology, Dalian 116012, People's Republic of China

[‡]Graduate School of Chinese Academy of Sciences, Beijing 100049, People's Republic of China

Supporting Information

ABSTRACT: Although cadmium has been recognized as a highly toxic heavy metal and poses many detrimental effects on human health, the Cd^{2+}-uptake and nosogenesis mechanisms are still insufficiently understood, mainly because of the lack of facile analytical methods for monitoring changes in the environmental and intracellular Cd^{2+} concentrations with high spatial and temporal reliability. To this end, we present the design, synthesis, and photophysical properties of a cadmium sensor, **DQCd1** based on the fluorophore 4-isobutoxy-6-(dimethylamino)-8-methoxyquinaldine (model compound **1**). Preliminary investigations indicate that **1** could be protonated under neutral media and yield a resonance process over the quinoline fluorophore. Upon excitation at 405 nm, **1** shows a strong fluorescence emission at 554 nm with a quantum yield of 0.17. Similarly, **DQCd1** bears properties comparable to its precursor. It exhibits fluorescence emission at 558 nm ($\Phi_f = 0.15$) originating from the monocationic species under physiological conditions. Coordination with Cd^{2+} causes quenching of the emission at 558 nm and simultaneously yields a significant hypsochromic shift of the emission maximum to 495 nm ($\Phi_f = 0.11$) due to inhibition of the resonance process. Thus, a single-excitation, dual-emission ratiometric measurement with a large blue shift in emission ($\Delta\lambda = 63$ nm) and remarkable changes in the ratio ($F_{495\ nm}/F_{558\ nm}$) of the emission intensity (R/R_0 up to 15-fold) is established. Moreover, the sensor **DQCd1** exhibits very high sensitivity for Cd^{2+} ($K_d = 41$ pM) and excellent selectivity response for Cd^{2+} over other heavy- and transition-metal ions and Na^+, K^+, Mg^{2+}, and Ca^{2+} at the millimolar level. Therefore, **DQCd1** can act as a ratiometric fluorescent sensor for Cd^{2+} through inhibition of the resonance process. Confocal microscopy and cytotoxicity experiments indicate that **DQCd1** is cell-permeable and noncytotoxic under our experimental conditions. It can indeed visualize the changes of intracellular Cd^{2+} in living cells using dual-emission ratiometry.

INTRODUCTION

Cadmium (Cd) and its derivatives are extremely toxic, and their bioaccumulations, consequently, result in many serious diseases and even many types of cancers.[1] The EPA (United States Environmental Protection Agency) gives an enforceable drinking water standard for Cd of 5 ppb to prevent kidney damage and other related diseases, while the WHO (World Health Organization) provides a more strict guideline value for Cd of 3 ppb for drinking water.[2] Recent reports revealed that the multiple cytotoxic and metabolic effects of Cd may principally originate from interference with the normal functions of essential metals such as Zn^{2+} and Ca^{2+}.[3,4] Besides, Cd is also involved in inducing oxidative stress and altering the activities of various enzymes.[5] Although these delectable progresses in the disclosure of toxic effects of Cd have been achieved, the Cd^{2+}-uptake and nosogenesis mechanisms are still poorly understood.[6] Thus, it is highly desirable to develop reliable analytical techniques for detecting and monitoring Cd in drinking water, environmental samples, and cell/tissues so as to clarify the biological roles of Cd.

Recently, fluorescent sensors capable of optically sensing transition-metal ions have attracted increasing attention because of their simplicity, high sensitivity, and high resolution of fluoroscopy.[7] Historically, some fluorescent sensors for Cd^{2+} have been reported,[8] but only a few of them are applicable to cellular imaging.[9] Moreover, most of these sensors are intensity-based and do not provide sufficient accuracy for quantitative measurements because their emission intensity is known to be conditioned by many variables, such as the sample environment, sensor concentration, bleaching, and instrumental efficiency. In contrast, ratiometric sensors can eliminate most or all ambiguities by built-in calibration of the two emission bands.[10] To this end, several sensors have been developed and utilized in ratiometric Cd^{2+} imaging in living cells.[11] In spite of their fascinating responses to Cd^{2+}, these sensors still have some hangups, such as poor water solubility, UV excitation, and large spectral overlap, and should be refined further. To date, it is still a tremendous challenge to design Cd^{2+}-selective sensors, in particular, ratiometric sensors for the accurate detection of Cd^{2+} in aqueous solutions and biological environments.

Received: January 6, 2011
Published: March 11, 2011

Scheme 1. Resonance Process of the Protonated 4-Methoxyquinoline (Pyridine) Derivatives

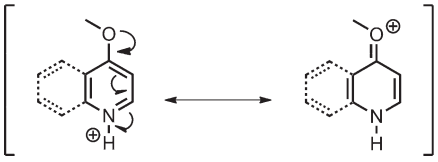

It is well-known that an essential resonance effect exists in protonated 4-alkoxy-substituted quinoline (pyridine) derivatives (Scheme 1).[12] The resonance charge transfer from the electron-donating methoxy group to the quinolinic (pyridinic) nitrogen would cause the charge to delocalize, resulting in a resonant oxonium electronic structure. Consequently, this resonance would greatly stabilize the conjugate acid and lead to a drastic red shift in the absorption wavelength. We speculate that a dye bearing such a feature can be utilized in the design of a sensor in which the signal readout is regulated by switching of the resonance process upon protonation or deprotonation. Therefore, we designed the model compound **1** (Scheme 2), which possesses the intramolecular charge-transfer pathway from the dimethylamino group to the quinolinic nitrogen, and expected that the quinolinic nitrogen would be protonated under neutral aqueous solutions because of the strengthened basicity originating from the presence of 6-dimethylamino and 4-isobutoxy groups.[12,13] So, a similar resonance would take place and stabilize the protonated species, consequently leading to long-wavelength absorption and fluorescence emission.

On the other hand, the di-2-picolylamine (DPA) moiety was initially employed for Zn^{2+}-selective sensors and has been widely investigated so far.[14] In fact, most of these Zn^{2+} sensors exhibit similar significant responses to Cd^{2+} as well because of the close chemical properties between Zn^{2+} and Cd^{2+}. However, when incorporated with auxiliary receptors, the DPA moiety is also available for the design of Cd^{2+}-selective sensors with preserved superiorities such as a high affinity for Cd^{2+} and fast Cd complex formation, high selectivity for Cd^{2+} over Ca^{2+}, Mg^{2+}, Na^{+}, and K^{+}, and good membrane permeability.[11,15] When such a chelator, which would create a metal-ion binding pocket with participation of the quinolinic nitrogen atom, is incorporated into model compound **1** to obtain the sensor **DQCd1**, the resonance process of the protonated **DQCd1** can be turned off by coordination-induced deprotonation of **DQCd1**. Consequently, inhibition of resonance and charge delocalization causes a distinct blue-shift fluorescence emission and provides a single-excitation, dual-emission ratiometric measurement for metal cations.

RESULTS AND DISCUSSION

Synthesis. The synthetic strategies for preparing **1**, **1**·HCl, and **DQCd1** are outlined in Scheme 3. The starting compound was initially protected with acetic anhydride in 92% yield to generate **2**. The reduction of the nitro group in **2** to an amino group by hydrogenation using Pd/C was efficient and afforded the quantitative product of **3**. Compound **4** was prepared by alkylation of **3** with formaldehyde and sodium borohydride in acidic media (yield 89%)[16] and further deprotected to achieve the *o*-anisidine precursor **5**. The enamine **6**, which was prepared by condensation of the *o*-anisidine **5** with ethyl acetoacetate, was cyclized thermally (reflux of diphenyl oxide) under nitrogen to give quinolone **7** (yield of about 71%). Although an attempt to alkylate the 4-position oxygen of **7** through the Mitsunobu

Scheme 2. Design Strategy for 1 and DQCd1

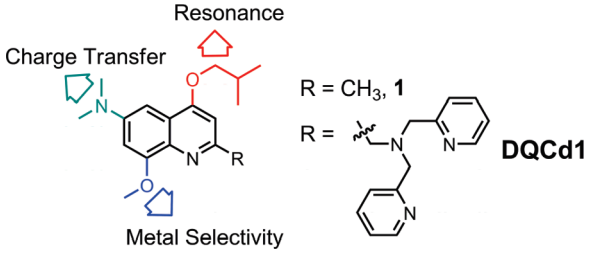

reaction failed, direct O-alkylation using 1-iodo-2-methylpropane under basic conditions produced model compound **1** in moderate yield. Then the hydrochloric salt of **1** was obtained by acidification of **1** with HCl (1 M). Compound **1** was further oxidized to generate aldehyde **8**, which was combined with DPA in dry 1,2-dichloroethane in the presence of $NaB(OAc)_3H$ to give **DQCd1** in reasonable yield after column chromatography and recrystallization. Finally, the metal complexes of **DQCd1** were obtained through the reaction of **DQCd1** with $Zn(NO_3)_2$ and $CdCl_2$. Suitable single crystals for X-ray crystallography were obtained by solvent diffusion.

Resonance in 1 and DQCd1. We first studied the photophysical properties of model compound **1**. The fluorescence spectra show that emission of **1** remains constant in a wide pH range from 4 to 7 and is quenched gradually as the pH reaches 9. Clearly, two protonation/deprotonation events affect the fluorescence emission. According to the similar protonation/deprotonation steps of 6-(dimethylamino)quinaldine (**6-DQ**)[13] with pK_{a1} = 6.8 (ring nitrogen) and pK_{a2} = 1.9 (exocyclic nitrogen), the apparent pK_a values of 7.67 and 2.46 (Figure 1) for **1** can be assigned to the nitrogen atoms at the quinolinic ring and amino group, respectively. On the other hand, the pK_a values of 7.61 and 2.41 obtained from UV−vis measurements are very similar to those based on fluorometric experiments (Figure S3 in the Supporting Information). These pK_a values indicate that protonation of **1** takes place under neutral aqueous media in the ground state. It should be noted that in contrast to the pK_a values of **6-DQ**, compound **1** shows a stronger tendency to form monoprotonated species at neutral media. This basicity-strengthening effect could be explained as the existence of resonance over the quinolinic fluorophore. Such a resonance process was further confirmed by theoretical calculations. Density functional theory (DFT) computations reveal that the positive charge of the monoprotonated species distributes over the isobutoxy group and quinolinic nitrogen. Further, ^1H NMR studies also demonstrate that the CH_2 signal of the isobutoxy proton in **1** undergoes a remarkable downfield shift ($\Delta\delta$ = 0.29 ppm) upon protonation (see NMR section), clearly indicating the presence of a partial positive charge on the isobutoxy group and the existence of resonance. In addition, the DFT calculations also suggest that the energy of the $S_0 \rightarrow S_1$ transition of the protonated species is much lower than that of neutral species (Supporting Information), consistent with the large red shift in the experimental absorption wavelength (~400 nm). Upon excitation at 405 nm, **1** shows a strong fluorescence emission at 554 nm with a quantum yield of 0.17 in aqueous solutions (pH = 7.4).

Next, we were encouraged to investigate the effect of pH on UV−vis absorption and fluorescence emission of **DQCd1** (Figures 1 and S4 in the Supporting Information). Although

dx.doi.org/10.1021/ic200032e |*Inorg. Chem.* 2011, 50, 3680–3690

Scheme 3. Synthetic Strategy for 1, 1·HCl, and DQCd1[a]

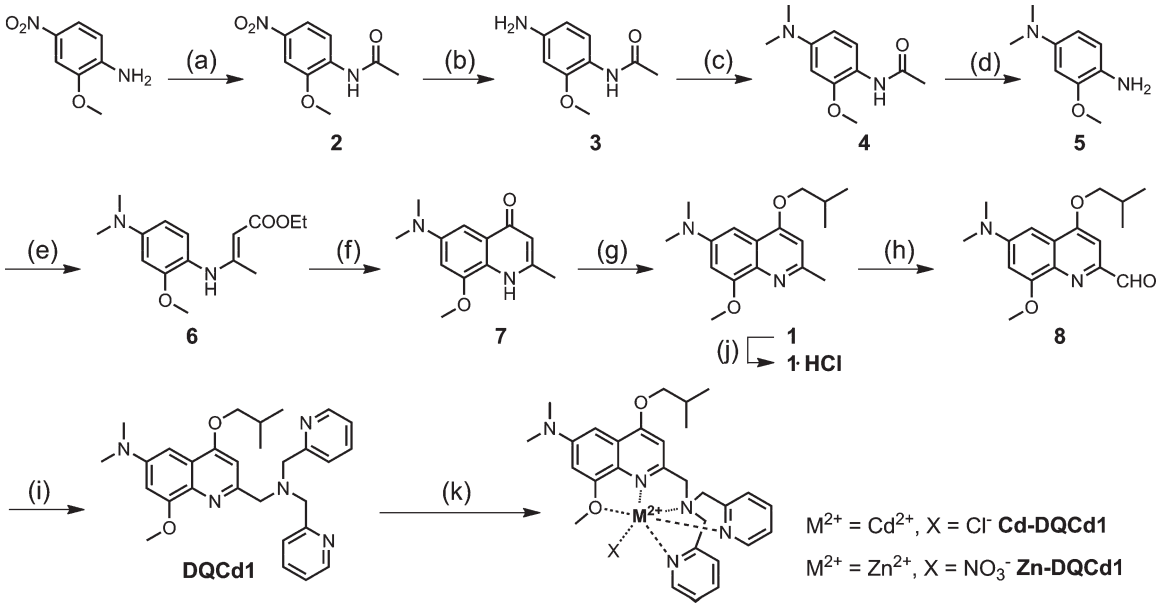

[a] Reagents and conditions: (a) Ac_2O, pyridine, 120 °C, 92%. (b) H_2, Pd/C, EA, rt, >95%. (c) 40% aqueous HCHO, $NaBH_4$, THF/H_2SO_4, 0 °C, 89%. (d) H_2SO_4, MeOH, 60 °C, >95%. (e) Ethyl acetoacetate, AcOH, benzene, reflux, 60%. (f) Diphenyl oxide, 250 °C, 71%. (g) 1-Iodo-2-methylpropane, K_2CO_3, DMF, 80 °C, 60%. (h) SeO_2, dioxane, 80 °C, 57%. (i) DPA, $NaBH(AcO)_3$, rt, 90%. (j) EtOH, HCl (1.0 M), rt, 91%. (k) $CdCl_2$ or $Zn(NO_3)_2$, MeOH, rt.

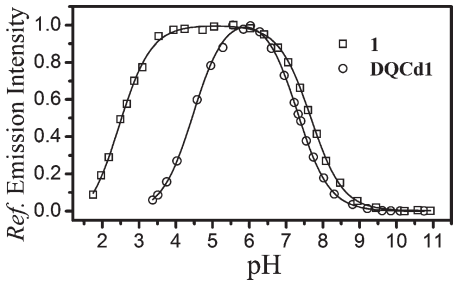

Figure 1. (a) Normalized emission intensity of **1** (□, λ_{em} = 554 nm) and **DQCd1** (○, λ_{em} = 558 nm) in aqueous buffer (10 mM HEPES and 0.1 M NaCl); λ_{ex} = 405 nm. The solid lines represent the nonlinear least-squares fits to the experimental data.

the DPA-based **DQCd1** bears multiple potential protonation sites, indeed, we only found two protonation/deprotonation processes from our photometric experiments, which have apparent pK_a values of 7.31 and 4.46 (7.45 and 4.65) from the fluorescence (UV−vis) spectra. According to the model compound **1**, the larger pK_a was assigned to the quinolinic nitrogen, but the smaller one was assigned to one of 2-pyridyl arms rather than the dimethylamino nitrogen.[17] The pK_{a1} (7.31) of **DQCd1** is about 0.4 unit lower in comparison with that (7.67) of **1**, suggesting a weaker basic site of the quinolinic nitrogen. We speculated that the quinolinic nitrogen, the tertiary nitrogen, 2-pyridyl groups of DPA, and the methoxy group constituted a binding pocket that was occupied by a proton (Scheme 4). This implies that the quinolinic nitrogen is not the sole site of protonation and the tertiary amine and pyridine groups are also involved in protonation, which, in turn, inhibits the photoinduced electron-transfer quenching effect of tertiary amine. Thus, **DQCd1** exhibits relatively high fluorescence emission (Φ_f = 0.15). In addition, the 2-pyridyl groups also participate in hydrogen bonding as acceptors for the proton so that the nearby positive charge originating from the proton binding pocket results in a smaller pK_a (4.46) of the pyridine moiety in **DQCd1** than that of free pyridine (5.17).[18] This similar pocketlike binding environment for the proton was also proposed for fluorescein-DPA-based sensors by Lippard et al.[17] These findings demonstrate that **DQCd1** can be protonated under physiological conditions and displays a resonance process similar to that of model compound **1**.

Optical Responses of DQCd1 to Cd^{2+}. With these data on hand, we chose a 10 mM HEPES, 0.1 M NaCl, pH = 7.4 aqueous buffer for investigating the abilities of **DQCd1** to sense Cd^{2+} (Table 1). In this solution, **DQCd1** showed a good solubility and stable photophysical properties even after 25 days (Figure S5 and S6 in the Supporting Information). The absorption spectra of free **DQCd1** showed a clear charge-transfer band around 420 nm ($\varepsilon = 1.9 \times 10^3\ M^{-1}\ cm^{-1}$), resulting from its monoprotonated species. Upon the addition of Cd^{2+}, this band decreased gradually, accompanied by a new blue-shift band around 370 nm with five distinct isosbestic points at 388, 348, 335, 311, and 277 nm (Figure 2a), implying a different coordination process between quinoline fluorophore and Cd^{2+} from its analogues.[15b,19] The saturated spectra were readily obtained when 1 equiv of Cd^{2+} was introduced, suggesting a strong affinity for Cd^{2+} and the formation of a 1:1 complex (Figure 2a, inset), which was further confirmed by Job's plots, ^1H NMR titration experiments, and X-ray crystallographic analysis (Figures 3, 6, and S7 in the Supporting Information). The free ligand shows a strong fluorescence emission at 558 nm with a quantum yield Φ_f of 0.15 upon excitation at 405 nm. Titration of **DQCd1** with Cd^{2+} caused quenching of the emission at 558 nm. Simultaneously, a new blue-shift emission band appeared at 495 nm with a large hypsochromic shift of 63 nm and a distinct isoemission point at 528 nm (Figure 2b).

dx.doi.org/10.1021/ic200032e |*Inorg. Chem.* 2011, 50, 3680–3690

Scheme 4. Chemical Equilibria of DQCd1 To Form Protonated and Metal-Bound Complexes

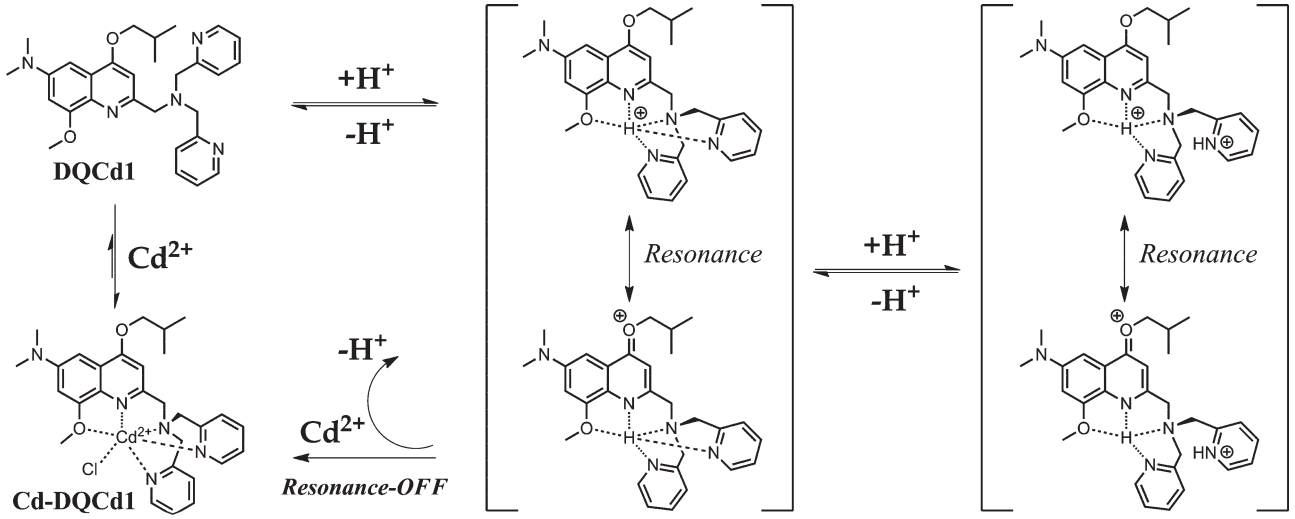

Table 1. Spectroscopic Data for the Compounds[a]

compound	λ_{abs}[b] [nm]	$\varepsilon \times 10^4$ [M^{-1} cm^{-1}]	λ_{em}[b] [nm]	Φ_f[c]
1	252	2.88	554	0.17
DQCd1	258	3.74	558	0.15
Cd-DQCd1	262	4.80	495	0.11
Zn-DQCd1	263	4.34	510	0.06

[a] 10 mM HEPES, 0.1 M NaCl, pH = 7.4, 25 °C. [b] The maximum absorption or emission intensity. [c] Quinine sulfate was used as the standard for quantum yield measurements.

The quantum yield of **DQCd1** was found to be 0.11 in the presence of 1 equiv of Cd^{2+}. The ratios of the fluorescence intensities at 495 and 558 nm were found to be 0.2 and 3.1 in the absence and presence of Cd^{2+}, respectively, indicating that **DQCd1** is an excellent dual-emission ratiometric fluorescent sensor for Cd^{2+} (R/R_0 up to 15). These results also demonstrate that the proton at the quinolinic site of **DQCd1** was displaced by Cd^{2+} because of strong coordination between Cd^{2+} and **DQCd1**, consequently resulting in inhibition of resonance and affording a ratiometric approach to the detection of Cd^{2+} (Scheme 4). Thus, **DQCd1** exhibits a large blue shift in emission and a remarkable increase in the intensity ratio ($F_{495\ nm}/F_{558\ nm}$) upon binding to Cd^{2+} and provides a good opportunity to generate high-resolution images for cellular Cd^{2+} using dual-emission ratiometry.

^{1}H NMR Studies. The protonation and metal-ion coordination events were further investigated by ^{1}H NMR data in deuterated dimethyl sufloxide (DMSO-d_6; Figure 3), and assignments of the proton signals are based on ^{1}H−^{1}H COSY and HMBC experiments (see the Supporting Information). We first obtained ^{1}H NMR spectra of **1** and **1**·HCl. As shown in Figure 3a, protons H(1′) and H(9′) display remarkable downfield shifts up to $\Delta\delta$ = 0.59 and 0.29 ppm upon protonation, respectively, hinting at the existence of a positive charge at the quinoline nitrogen. Notably, the chemical shift of the proton H(6′) of the isobutoxy group also underwent a significant downfield shift from 3.95 to 4.24 ppm ($\Delta\delta$ = 0.29 ppm), which clearly shows delocalization of the partial positive charge on the oxygen atom, substantially confirming the existence of resonance. Next, we examined the metal binding of **DQCd1** (Figure 3b). The remarkable proton shifts of the DPA moiety and the 3-position proton H(1′) indicate that Cd^{2+} coordinated to the DPA moiety and the quinoline fluorophore. Interestingly, the chemical shift of the proton H(1′) displayed an upfield shift, and the isobutoxy H(6′) showed a slight downfield shift upon the addition of Cd^{2+}. These results indicate that charge distribution of the butoxy oxygen is less affected by Cd^{2+} coordination to the quinolinic nitrogen atom, and the resonance effect does not take

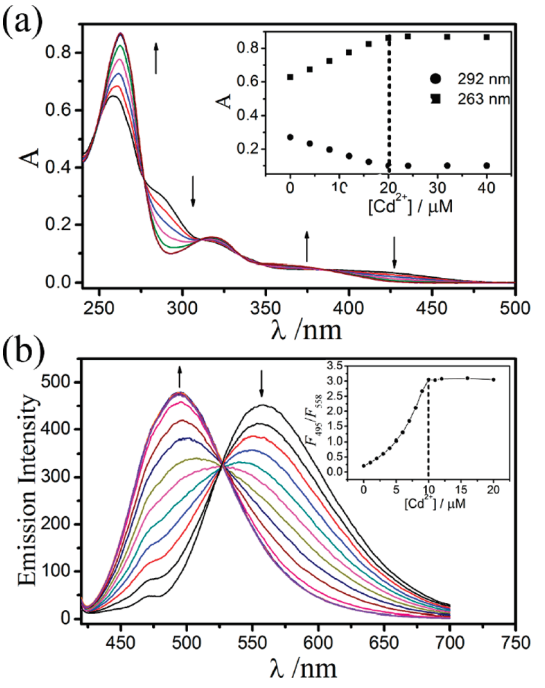

Figure 2. (a) Absorption spectra of 20 μM **DQCd1** upon titration of Cd^{2+} (0−40 μM) in aqueous buffer (10 mM HEPES, 0.1 M NaCl, pH = 7.4). Inset: Absorbance changes as a function of the Cd^{2+} concentration. (b) Fluorescence spectra (λ_{ex} = 405 nm) of 10 μM **DQCd1** upon titration of Cd^{2+} (0−20 μM) in aqueous buffer. Inset: Ratio ($F_{495\ nm}/F_{558\ nm}$) changes as a function of the Cd^{2+} concentration.

dx.doi.org/10.1021/ic200032e |*Inorg. Chem.* 2011, 50, 3680–3690

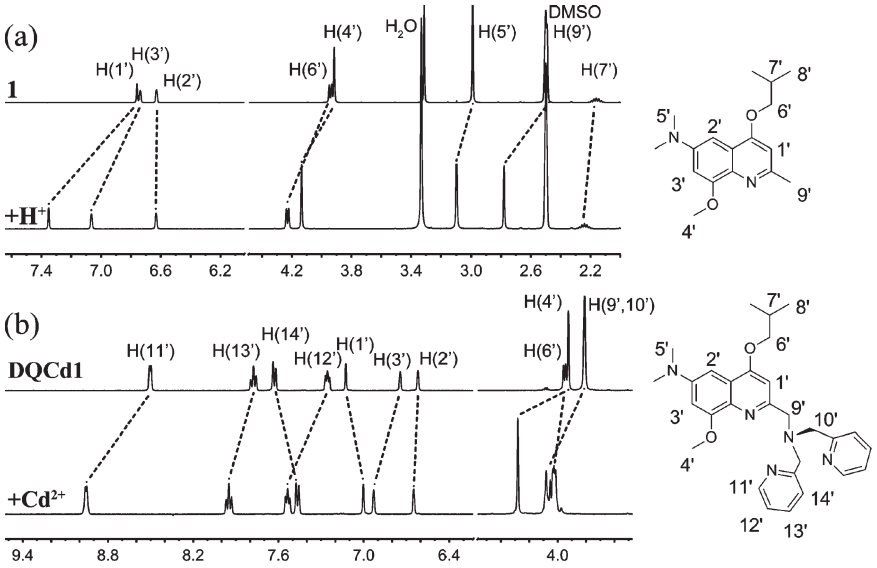

Figure 3. Partial ^{1}H NMR spectra (400 MHz) of (a) **1** (5 mM) and **1**·HCl (5 mM). (b) **DQCd1** (5 mM) and **DQCd1** + Cd^{2+} (5 mM) in DMSO-d_6.

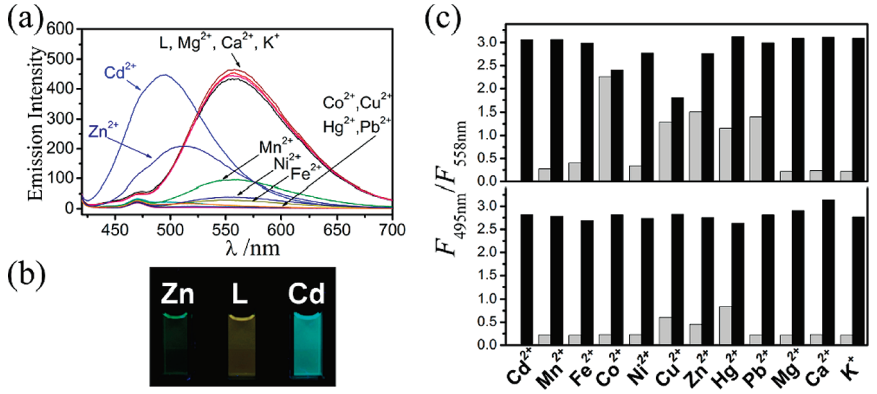

Figure 4. (a) Fluorescence spectra of **DQCd1** (10 μM) in the presence of various metal ions (10 μM Mn^{2+}, Fe^{2+}, Co^{2+}, Ni^{2+}, Cu^{2+}, Zn^{2+}, Cd^{2+}, Hg^{2+}, and Pb^{2+} and 1 mM Mg^{2+}, Ca^{2+}, and K^+) in a buffer solution (10 mM HEPES, 0.1 M NaCl, pH = 7.4, λ_{ex} = 405 nm). (b) Visible emission observed from samples of **DQCd1** (L), **Cd-DQCd1**, and **Zn-DQCd1**, λ_{ex} = 365 nm. (c) Metal-ion selectivity profiles of **DQCd1** (10 μM) in the absence (top) and presence (bottom) of 50 μM NTA. Gray bars represent the fluorescence intensity ratio responses ($F_{495\ nm}/F_{558\ nm}$) of **DQCd1** in the presence of various metal ions. Black bars represent the ratio responses of **DQCd1** in the presence of the indicated metal ions, followed by 10 μM Cd^{2+}.

place because of the strong electron-withdrawing effect of the metal ion.

Metal-Ion Selectivity. The selectivity profiles of **DQCd1** were examined by titrations with various potential competing metal ions (Figure 4). Na^+, K^+, Ca^{2+}, and Mg^{2+}, which are abundant in water and living samples, exerted a negligible effect on the fluorescence response for Cd^{2+} even at high concentrations (1 mM). Co^{2+}, Ni^{2+}, and Cu^{2+} strongly quenched the fluorescence (Figures 4a and S8a in the Supporting Information), even in the presence of an equal equivalent of Cd^{2+}. Zn^{2+} partially quenched the emission of **DQCd1** (Φ_{Zn} = 0.055) but with a new emission at 510 nm and a smaller hypsochromic shift ($\Delta\lambda$ = 48 nm) than that of Cd^{2+}. These results indicate that **DQCd1** is able to distinguish Cd^{2+} from Zn^{2+} by both fluorescence emission wavelength and intensity upon metal binding, even by "naked eyes" (Figure 4b). Adding Cd^{2+} to a **Zn-DQCd1** solution caused a rapid increase in both the fluorescence intensity and the ratio signals within 10 min (Figure S8 in the Supporting Information), implying that Zn^{2+} has little interference on Cd^{2+} sensing. In fact, in some more complicated systems, such as seawater and biological samples, the practicability for detection of Cd^{2+} may be diminished by the high level of other 3d metal ions, especially for Zn^{2+}. To further eliminate this interference, we chose nitrilotriacetic acid (NTA) as a masking agent because NTA has higher affinities for Zn^{2+} (log K_{Zn} = 10.66) than those for Cd^{2+} (log K_{Cd} = 9.78).[20] So, selectivity experiments were repeated in the presence of 5 equiv of NTA under otherwise identical conditions. Although Zn^{2+} and other transition-metal ions (Mn^{2+}, Fe^{2+}, Co^{2+}, Ni^{2+}, Cu^{2+}, Hg^{2+}, and Pb^{2+}) result in the partial quenching of fluorescence but without a distinct blue shift (Figure S9 in the Supporting Information), the ratio values of $F_{495\ nm}$ to $F_{558\ nm}$ (Figure 4c, bottom, gray bars) are much smaller than those in the absence of NTA (Figure 4c, top, gray bars). As expected, only Cd^{2+} induced an obvious blue shift of the emission and a significant increase in the ratio. The R/R_0 value of 13.5 is comparable with that in the absence of NTA (R/R_0 = 15). Moreover, the Cd^{2+}-induced ratio value ($F_{495\ nm}/F_{558\ nm}$) was not affected by the presence of the

dx.doi.org/10.1021/ic200032e |Inorg. Chem. 2011, 50, 3680–3690

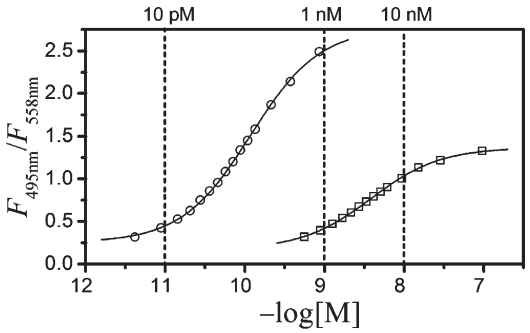

Figure 5. Ratio fluorescence responses ($F_{495\ nm}/F_{558\ nm}$) of **DQCd1** as a function of free Cd^{2+} (○) or Zn^{2+} (□) concentrations (M = Cd^{2+} or Zn^{2+}). The solid lines represent nonlinear least-squares fits to the experimental data.

above-mentioned metal ions (Figure 4c, bottom, black bars). Further experiments showed that, even in the media with an NTA concentration of 0.5 mM, 0.1 mM Zn^{2+} did not seriously interfere with the response ($R/R_0 \approx 10$) of **DQCd1** to Cd^{2+} at the micromolar level (Figure S10 in the Supporting Information). These data indicate that NTA can eliminate unfavorable effects of other transition metals, in particular Zn^{2+}, on the response of **DQCd1** to Cd^{2+}. Moreover, the related ratio value ($R = F_{495\ nm}/F_{558\ nm}$) of **DQCd1** and **Cd-DQCd1** showed a pH independence in the range of 6−8 (Figure S12 in the Supporting Information). Thus, **DQCd1** is suitable for monitoring intracellular Cd^{2+} based on the ratiometric assay under physiological conditions.

Binding Affinities. The accession of fluorescent molecules with high binding affinity is very important in the development of Cd^{2+}-selective sensors.[8h,11b,11c] It was shown that the Cd^{2+} concentrations are usually 1 ppb or even lower for unpolluted natural waters,[21,22] which are elevated by industrial discharge or contamination of municipal wastewater, and certain bioaccumulations in some shellfish take place in Cd^{2+}-contaminated seawater with a concentration as low as 10^{-7} M.[22] On the other hand, lower Cd^{2+} concentrations down to 100 pM were also found to significantly induce cell growth and DNA synthesis.[23] So, fluorescent sensors with dissociation constants (K_d values) in the subnanomolar or picomolar range will be practical to Cd^{2+} detection in these pools.

The dissociation constant of **DQCd1** for Cd^{2+} was determined by fluorescence spectroscopy in metal−ligand-buffered solutions with different Cd^{2+} concentrations. **DQCd1** responded to the picomolar concentration of free Cd^{2+}, and K_d was determined by using nonlinear least-squares fit analysis of the ratio of the fluorescence intensity ($F_{495\ nm}/F_{558\ nm}$; Figure 5) to be $4.1 \pm 0.3 \times 10^{-11}$ M (41 pM), indicating the high binding affinity of **DQCd1** for Cd^{2+}. The K_d value of **DQCd1** for Zn^{2+} was also calculated to be $1.3 \pm 0.1 \times 10^{-9}$ M, which is similar with that of the previously reported sensor **HQ1**.[19] These findings indicate that the 8-position methoxy group is propitious to binding Cd^{2+}, as observed in other 8-methoxyquinoline-based sensors.[8b,d,f,15b,19] Thus, we infer that the larger Cd^{2+} (ionic radii $r^+ = 0.96$ Å for Cd^{2+} and $r^+ = 0.74$ Å for Zn^{2+}) may be more suitable for the coordination cavity in space, resulting in a stronger interaction between Cd^{2+} and the methoxy oxygen and a consequent high affinity. On the other hand, the zinc complex lacking a suitable ion radius may be easily disrupted by protic solvent molecules, and fluorescence of this complex is partially quenched by nonradiative deactivations via vibronic coupling with the vibrational states of O−H oscillators.[8f] Accordingly, Cd^{2+} and Zn^{2+} induced significantly different fluorescence responses in aqueous solution but comparable fluorescence responses in an aqueous acetonitrile solution (HEPES buffer with 50% CH_3CN; Figure S15 in the Supporting Information). Similar phenomena were also described by us and Liu et al.[8f,15b]

The limit of detection (LOD) of **DQCd1** for Cd^{2+} (Figure S13 in the Supporting Information) was further determined to be 9.6 pM (1.1 ng/L), which is far lower than the maximum limit for drinking water emphasized by the WHO and EPA. In contrast with the traditional approach for the detection of Cd^{2+} in the environment, such as anodic stripping voltammetry (LOD of 1 ng/L)[24] and atomic absorption spectrometry (LOD of 5 ng/L),[25] we believe that **DQCd1** affords sufficient sensitivity for the detection of a trace amount of Cd^{2+} in environmental samples.

Table 2. Selected Bond Distances (Å) for the Crystal Structures[a]

compound	Cd-DQCd1	Zn-DQCd1
M−N1	2.304(4)	2.0688(16)
M−N2	2.457(4)	2.2089(16)
M−N3	2.352(5)	2.0993(16)
M−N4	2.278(5)	2.1444(15)
M−O1	2.647(4)	2.4939(14)
M−X	2.4472(17)	2.0587(15)

[a] M represents the metal ion Cd(2) or Zn(1); X represents the solvent molecule coordinated to the metal ion.

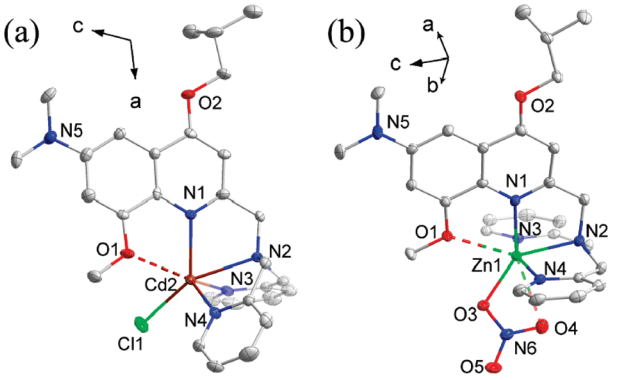

Figure 6. Crystal structures of the complexes (a) **Cd-DQCd1** and (b) **Zn-DQCd1**. Thermal ellipsoids are shown at the 50% probability level. All hydrogen atoms and counteranions are omitted for clarity.

X-ray Crystallographic Analysis. The solid states of metal complexes of **DQCd1** were investigated by X-ray crystallography. Initially, we attempted to crystallize various metal salts [MCl_2, MSO_4, $M(ClO_4)_2$, $M(NO_3)_2$, where M = Cd^{2+} or Zn^{2+}] with **DQCd1** in a variety of solvents. Indeed, the crystals suitable for crystallographic analysis were obtained in methanol/ethyl ether[26] and methanol/ethyl ether/H_2O[27] for **Cd-DQCd1** and **Zn-DQCd1**, respectively. The crystal structures and data of both complexes are shown in Figure 6, Table 2, and the Supporting Information. In the Cd complex **Cd-DQCd1**, each asymmetric unit contains two similar Cd coordination sets, where Cd^{2+} is chelated by quinoline, a chloride anion, and the DPA moiety to form a disordered trigonal-bipyramidal coordination geometry. Meanwhile, the distance between methoxy O1 and Cd2 of

dx.doi.org/10.1021/ic200032e |Inorg. Chem. 2011, 50, 3680–3690

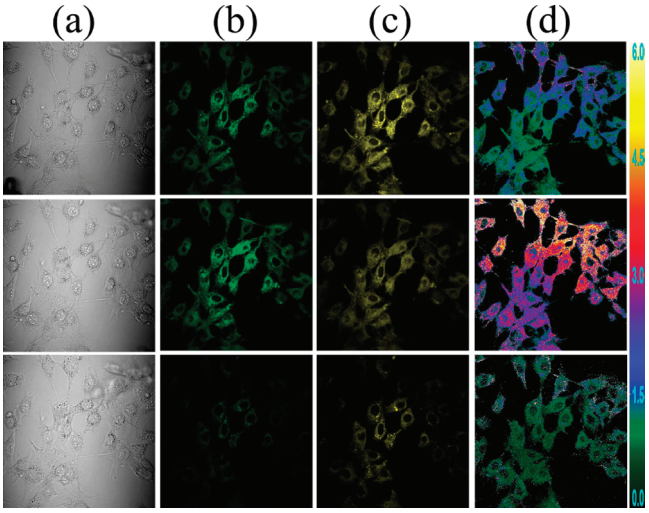

Figure 7. Confocal fluorescence images of intracellular Cd^{2+} in NIH 3T3 cells with 10 μM **DQCd1** in a PBS buffer: NIH 3T3 cells incubated with **DQCd1** (10 μM) at 37 °C for 30 min (top); **DQCd1**-stained cells exposed to 30 μM $CdCl_2$ at 25 °C for 25 min (middle); sequestration of intracellular Cd^{2+} by the addition of 50 μM TPEN (bottom). (a) Bright-field images. (b) Fluorescence images with emission collected at 430−490 nm. (c) Fluorescence images with emission collected at 530−590 nm. (d) Ratio images generated from parts b and c, $F_{430-490\ nm}/F_{530-590\ nm}$.

2.647(4) Å is obviously longer than that of a typical Cd−O bond, indicative of a weak coordination effect. Zn^{2+} adopts a similar coordination geometry in **Zn-DQCd1**, except that a nitrate anion instead of a chloride anion is coordinated to Zn^{2+}. The methoxy oxygen also undergoes weak interaction to Zn^{2+} with a Zn1···O1 distance of 2.494(4) Å, as is observed in its analogues in which the distance can reach as long as 2.688(4) Å.[19] However, the M−N coordination bonds fit the typical bond ranges in both complexes.[28] These data demonstrate that the DPA moiety plays the main function of grasping the metal ions, while the 8-position methoxy oxygen can be used to tune the selectivity of the sensor.

Ratiometric Fluorescence Imaging of Cd^{2+} in Living Cells. The cytotoxicity of the sensor is very essential with respect to the potential studies on the toxicity effect of Cd^{2+}. So, we measured the viability of the **DQCd1**-treated NIH 3T3 cells by the CCK-8 assay. The cytotoxicity measurements demonstrate that **DQCd1** is nontoxic up to 10 μM over at least a 24-h period (Table S5 in the Supporting Information). To further evaluate whether the sensing properties of **DQCd1** toward Cd^{2+} in vitro are preserved in intracellular conditions, we chose two different cell lines, NIH 3T3 (murine fibroblast cell line, a fibroblast cell) and HEK293 (human embryonic kidney cell line, an epithelial cell) to determine exogenous Cd^{2+} in living cells by using fluorescence microscopy.

NIH 3T3 cells, which were incubated with 10 μM **DQCd1** for 30 min in a phosphate-buffered saline (PBS) buffer at 37 °C and washed, showed clear intracellular fluorescence at an emission channel collected at 530−590 nm, indicating that **DQCd1** is cell-permeable (Figure 7). Costaining experiments with the commercial acidotropic dye LysoTracker Red (1 μM) confirm that **DQCd1** located at the acidic compartments of the cells shows the stronger fluorescence (Figure S16 in the Supporting Information). When the cells were treated with 30 μM $CdCl_2$ at 25 °C for 25 min, the intensity of the emission collected at

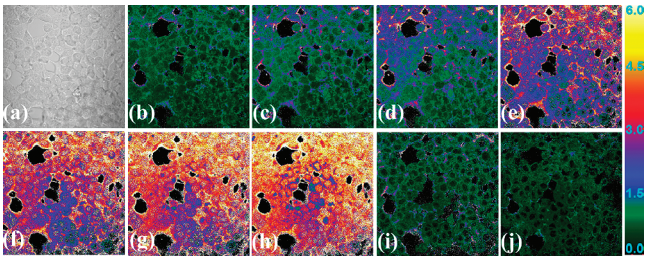

Figure 8. Fluorescence ratio images of Cd^{2+} in HEK 293 cells labeled with 10 μM **DQCd1** in PBS buffer. (a) Bright-field image. (b) Ratio image of emission window $F_{430-490\ nm}/F_{530-590\ nm}$. (c−h) Time-lapse ratio imaging of the cells after treatment with 30 μM $CdCl_2$ over 1 h. (i and j) Ratio images after treatment with 50 μM TPEN for 5 and 10 min.

530−590 nm decreased, whereas the intensity of the emission collected at 430−490 nm increased (Figure 7, middle). Accordingly, significant enhancement in the ratio of $F_{430-490\ nm}$ to $F_{530-590\ nm}$ can be obtained (Figure 7d). These are consistent with the observations in aqueous buffer and demonstrate that **DQCd1** can readily reveal variation of the intracellular Cd^{2+} concentrations (Figure 7, middle). Moreover, variations in fluorescence could be reversed by the subsequent addition of a 50 μM membrane-permeable chelator *N*,*N*,*N*′,*N*′-tetrakis(2-pyridylmethyl)ethylenediamine (TPEN) into the medium, indicating that an increase in the ratio of the emission originating from the response of **DQCd1** to intracellular Cd^{2+} (Figure 7, bottom). We further carried out confocal experiments in HEK 293 cells with **DQCd1**. As shown in Figures 8 and S17 in the Supporting Information, the ratio of $F_{430-490\ nm}$ to $F_{530-590\ nm}$ gradually increased after treatment of $CdCl_2$ and remained almost unchanged after 40 min. Similarly, the changes in the ratios were recovered by subsequent TPEN treatment. The data obtained from two cell lines demonstrate that **DQCd1** is able to visualize the explicit alteration of intracellular Cd^{2+} through the ratio images, which is obviously superior to intensity-based images of the sole emission channel.

■ CONCLUSION

We have investigated the absorption and fluorescence emission properties of two quinoline derivatives, **1** and **DQCd1**, and find that **1** and **DQCd1** with 4-isobutoxy groups can be protonated in aqueous solutions and thus generate the resonance process. We further demonstrated our strategy on the development of the fluorescent ratiometric sensor, **DQCd1**, by utilizing cation-induced inhibition of the resonance process. Such a sensor provides a single-excitation, dual-emission ratiometric detection of Cd^{2+} with a significant blue shift in emission and remarkable changes in the ratio ($F_{495\ nm}/F_{558\ nm}$) of the emission intensity. Moreover, the cell-permeable and noncytotoxic **DQCd1** can indeed visualize the changes of intracellular Cd^{2+} in living cells. It can thus be predicted that the design strategy of cation-induced inhibition of the resonance process allows one to design new ratiometric sensors for other metal ions of biological interest.

■ EXPERIMENTAL SECTION

Materials and Methods. Unless otherwise noted, materials were obtained from Alfa Aesar and were used without further purification. Di-2-picolylamine (DPA) was purchased from J&K Chemical Ltd. LysoTracker Red DND-99 was purchased from Invitrogen. All solvents were

purified and dried by standard methods prior to use. Pure water (18.2 Ω) was used to prepare all aqueous solutions. Melting points were measured using an X-4 melting point apparatus with a microscope. ^{1}H and ^{13}C NMR spectra were recorded using a Bruker AVANCE-400 400 MHz spectrometer. Two-dimensional NMR experiments were taken on a Bruker AVANCE-600 (600 MHz) spectrometer. Chemical shifts are expressed in parts per million (δ) using residual solvent protons as internal standards. IR data were recorded on a Bruker Tensor-27 spectrometer. Mass spectra (electrospray ionization, ESI) and high-resolution mass spectra (ESI) were obtained on LC-MS 2010 and Bruker Apex IV Fourier transform mass spectrometers, respectively. Elemental analyses were performed on a Vario EL analyzer (Elementar Analysensysteme GmbH). UV−vis absorption spectra were obtained using a Hitachi 3010 UV−vis spectrometer. Fluorescence spectra were obtained using a Hitachi F-4600 spectrometer.

Synthesis of Compound 2. A total of 10 g of 2-methoxy-4-nitroaniline and 2 equiv of acetic anhydride (11.5 mL) in 35 mL of pyridine was heated in a round-bottomed flask (100 mL) for 2 h at 120 °C. The solvent was evaporated under vacuum and azeotroped with toluene (twice) to generate a crude solid, which was purified by recrystallization from methanol to give the desired products as a yellow crystalline residue (11.5 g, 92%). TLC: R_f = 0.48 (silica, 1:1 petroleum ether/ethyl acetate). Mp: 157−158 °C. ^{1}H NMR (400 MHz, $CDCl_3$, ppm): δ 8.58 (d, J = 8.92 Hz, 1H), 7.96 (br s, 1H), 7.93 (d, J = 9.0 Hz, 1H), 7.75 (s, 1H), 4.00 (s, 3H), 2.26 (s, 3H). ^{13}C NMR (100 MHz, $CDCl_3$, ppm): δ 168.7, 147.2, 142.9, 133.9, 118.2, 117.6, 105.1, 56.3, 25.0. FTIR (KBr, cm^{-1}): 3281, 1675, 1590, 1510, 1338, 1284, 1096, 1027, 880, 801. MS (ESI): m/z 211.1 [M + H$^+$], 233.1 [M + Na$^+$]. ESI-HRMS. Calcd for [M + H$^+$] $C_9H_{11}N_2O_4$: m/z 211.0719. Found: m/z 211.0706. Calcd for [M + Na$^+$] $C_9H_{10}N_2NaO_4$: m/z 233.0538. Found: m/z 233.0526.

Synthesis of Compound 3. A solution of compound **2** (1.06 g, 5 mmol) in dry ethyl acetate (30 mL) was stirred at room temperature with 0.1 g of 5% Pd/C. After 8 h, the mixture was filtered off and the crude product was filtered on Celite and rinsed with ethyl acetate. Compound **3** was obtained as a purple oil and used without further purification. TLC: R_f = 0.21 (silica, 4:1 CH_2Cl_2/ethyl acetate). ^{1}H NMR (400 MHz, $CDCl_3$, ppm): δ 8.04 (d, J = 8.36 Hz, 1H), 7.45 (br, 1H), 6.28−6.25 (m, 2H), 3.81 (s, 3H), 2.15 (s, 3H). ^{13}C NMR (100 MHz, $CDCl_3$, ppm): δ 167.8, 149.3, 143.3, 121.7, 119.6, 107.1, 98.5, 55.7, 24.8. MS (ESI): m/z 181.1 [M + H$^+$], 203.1 [M + Na$^+$].

Synthesis of Compound 4. A slurry of compound **3** (0.9 g, 5 mmol) and finely crushed sodium borohydride (1.9 g, 50 mmol) in tetrahydrofuran (THF; 8 mL) was added to a stirred mixture of 3 M H_2SO_4 (2 mL) and 40% aqueous formaldehyde in an Erlenmeyer flask at a rate compatible with temperature control (0 ± 5 °C). After the addition was complete, the mixture was made strongly basic with solid sodium hydroxide and was extracted with ethyl acetate (20 mL × 3). The organic solutions were combined, washed with water and brine, and dried with Na_2SO_4. The solvents were evaporated to give the crude product, which was purified by flash chromatography (silica gel, CH_2Cl_2/5−10% ethyl acetate) to give the desired products as a white solid (0.93 g, 89% based on compound **2**). TLC: R_f = 0.5 (silica, 4:1 CH_2Cl_2/ethyl acetate). Mp: 113−114 °C. ^{1}H NMR (400 MHz, $CDCl_3$, ppm): δ 8.11 (d, J = 8.76 Hz, 1H), 7.45 (br s, 1H), 6.33−6.3 (m, 2H), 3.87 (s, 3H), 2.92 (s, 6H), 2.16 (s, 3H). ^{13}C NMR (100 MHz, $CDCl_3$, ppm): δ 167.7, 149.3, 148.1, 121.4, 118.1, 104.8, 96.3, 55.5, 41.0, 24.6. FTIR (KBr, cm^{-1}): 3273, 2994, 2888, 2809, 1647, 1534, 1484, 1420, 1362, 1323, 1130, 1031, 981, 805, 780, 602, 518, 459. MS (ESI): m/z 209.1 [M + H$^+$], 231.1 [M + Na$^+$]. ESI-HRMS. Calcd for [M + H$^+$] $C_{11}H_{17}N_2O_2$: m/z 209.1290. Found: m/z 209.1278. Calcd for [M + Na$^+$] $C_{11}H_{16}N_2NaO_2$: m/z 231.1109. Found: m/z 231.1097.

Synthesis of Compound 5. Compound **4** (1.2 g, 6 mmol) was dissolved in 20 mL of MeOH. Then 1 mL of concentrated sulfuric acid was slowly added. The mixture was heated at 60 °C and was stirred for 4 h. The reaction mixture was cooled and neutralized with sodium hydroxide, and then CH_2Cl_2 (15 mL × 5) was added. The organic solutions were combined, washed with water and brine, and dried with Na_2SO_4. Compound **5** was obtained as a purple oil and used without further purification. TLC: R_f = 0.30 (silica, 25:1 CH_2Cl_2/MeOH). ^{1}H NMR (400 MHz, $CDCl_3$, ppm): δ 6.67 (d, J = 8.40 Hz, 1H), 6.40 (s, 1H), 6.30 (d, J = 6.40 Hz, 1H), 3.85 (s, 3H), 3.35 (br, 2H), 2.84 (s, 6H). ^{13}C NMR (100 MHz, $CDCl_3$, ppm): δ 148.4, 145.4, 127.9, 116.2, 106.7, 99.5, 55.5, 42.3. MS (ESI): m/z 167.1 [M + H$^+$].

Synthesis of Compound 6. A solution of compound **5** (1.0 g, 6 mmol), ethyl acetoacetate (1.6 g, 12 mmol), and AcOH (0.5 mL) in benzene (30 mL) was refluxed for 8 h, removing water with a Dean−Stark apparatus. This mixture was cooled to room temperature and concentrated in vacuum. The residue was purified by flash chromatography (silica gel, petroleum ether/0−10% ethyl acetate) to give the desired products as a white solid (1.0 g, 60% based on compound **4**). TLC: R_f = 0.40 (silica, 5:1 petroleum ether/ethyl acetate). Mp: 109−110 °C. ^{1}H NMR (400 MHz, $CDCl_3$, ppm): δ 9.86 (s, 1H), 6.96 (d, J = 8.40 Hz, 1H), 6.27 (br, 2H), 4.63 (s, 1H), 4.17 (q, J = 7.08 Hz, 2H), 3.83 (s, 3H), 2.96 (s, 6H), 1.85 (s, 3H), 1.28 (t, J = 7.08 Hz, 3H). ^{13}C NMR (100 MHz, $CDCl_3$, ppm): δ 170.6, 161.4, 154.9, 150.1, 127.6, 117.9, 104.1, 96.7, 83.9, 58.5, 55.7, 40.9, 20.0, 14.8. FTIR (KBr, cm^{-1}): 3283, 2982, 2900, 2813, 1652, 1599, 1566, 1523, 1492, 1442, 1387, 1362, 1262, 1161, 1060, 1034, 978, 805, 782, 659, 543. MS (ESI): m/z 279.2 [M + H$^+$]. ESI-HRMS. Calcd for [M + H$^+$] $C_{15}H_{23}N_2O_3$: m/z 279.1709. Found: m/z 279.1697. Calcd for [M + Na$^+$] $C_{15}H_{22}N_2NaO_3$: m/z 301.1528. Found: 305.1518. Calcd for [M + K$^+$] $C_{15}H_{22}N_2KO_3$: 317.1267. Found: 317.1258.

Synthesis of Compound 7. A mixture of compound **6** (1.00 g, 3.6 mmol) and diphenyl ether (15.0 g) was heated with stirring at 250 °C for 60 min under nitrogen. This mixture was cooled, and the product began to precipitate in the reaction medium. After cooling, the mixture was diluted with 100 mL of petroleum ether to complete the precipitation. The solid was filtered off, washed with ethyl acetate, and recrystallized from methanol to give of the product as a yellow crystalline residue (0.59 g, 71%). Mp: 272−273 °C. TLC: R_f = 0.37 (silica, 1:1 petroleum ether/isopropyl alcohol). ^{1}H NMR (400 MHz, DMSO-d_6, ppm): δ 10.78 (s, 1H), 6.77 (s, 2H), 5.78 (s, 1H), 3.98 (s, 3H), 2.94 (s, 6H), 2.32 (s, 3H). ^{13}C NMR (100 MHz, MeOD, ppm): δ 179.2, 150.6, 149.9, 149.1, 127.0, 125.0, 108.7, 101.0, 96.5, 56.4, 41.0, 19.6. FTIR (KBr, cm^{-1}): 3055, 2937, 2893, 1629, 1592, 1556, 1505, 1438, 1395, 1372, 1263, 1229, 1203, 1147, 1076, 997, 881, 845, 820, 762, 549, 532, 499. MS (ESI): m/z 233.2 [M + H$^+$]. ESI-HRMS. Calcd for [M + H$^+$] $C_{13}H_{17}N_2O_2$: m/z 233.1290. Found: m/z 233.1279.

Synthesis of Compound 1. A mixture of compound **7** (233 mg, 1 mmol), 1-iodo-2-methylpropane (220 mg, 1.2 mmol), and K_2CO_3 (0.55 g, 4 mmol) in *N*,*N*-dimethylformamide (DMF; 8 mL) was heated at 80 °C for 8 h. After cooling, H_2O (30 mL) was added to the mixture and extracted with ethyl acetate (10 mL × 3). The organic solutions were combined, washed with water and brine, and dried with Na_2SO_4. The solvents were evaporated to give the crude product, which was purified by flash chromatography (silica gel, CH_2Cl_2/0−30% acetone) to give the desired products as a pale-yellow solid (184 mg, 60%). TLC: R_f = 0.38 (silica, 25:2 CH_2Cl_2/MeOH). Mp: 135−136 °C. ^{1}H NMR (400 MHz, $CDCl_3$, ppm): δ 6.81 (s, 1H), 6.67 (s, 1H), 6.56 (s, 1H), 4.04 (s, 3H), 3.92 (d, J = 6.40 Hz, 2H), 3.05 (s, 6H), 2.67 (s, 3H), 2.26 (m, 1H), 1.12 (d, J = 6.56 Hz, 6H). ^{13}C NMR (100 MHz, $CDCl_3$, ppm): δ 160.5, 155.3, 155.0, 148.2, 135.0, 121.9, 102.0, 98.9, 92.7, 74.4, 55.9, 41.2, 28.3, 25.9, 19.5. FTIR (KBr, cm^{-1}): 2959, 2926, 2870, 2808, 1622, 1597, 1504, 1463, 1415, 1388, 1357, 1260, 1219, 1150, 1087, 998, 820, 777, 671, 645, 575. MS (ESI): m/z 289.2 [M + H$^+$]. ESI-HRMS. Calcd for [M + H$^+$] $C_{17}H_{25}N_2O_2$: m/z 289.1916. Found: m/z 289.1909. Anal.

Calcd for $C_{17}H_{26}N_2O_3$ (**1**·H_2O): C, 66.64; H, 8.55; N, 9.14. Found: C, 66.56; H, 8.47; N, 9.24.

Synthesis of Compound 1·HCl. A mixture of compound **1** (50 mg, 0.16 mmol), HCl (1 M, 0.16 mL), and EtOH (5 mL) was stirred at room temperature for 10 min. The solvents were evaporated to give a crude product, which was purified by recrystallization from ethyl acetate/CH_2Cl_2 to give the desired products as a yellow solid (54 mg, 91%). Mp: 182−183 °C. ^{1}H NMR (400 MHz, DMSO-d_6, ppm): δ 14.14 (s, 1H), 7.35 (s, 1H), 7.07 (s, 1H), 6.64 (s, 1H), 4.24 (d, J = 6.36 Hz, 2H), 4.14 (s, 3H), 3.10 (s, 6H), 2.78 (s, 3H), 2.24 (m, 1H), 1.09 (d, J = 6.56 Hz, 6H). FTIR (KBr, cm^{-1}): 2962, 2877, 2812, 1613, 1494, 1445, 1419, 1355, 1326, 1270, 1233, 1150, 1087, 989, 906, 878, 831, 809, 757, 635, 584. ESI-HRMS. Calcd for $C_{17}H_{25}N_2O_2$: m/z 289.1916. Found: m/z 289.1904. Anal. Calcd for $C_{17}H_{30}N_2O_{4.5}Cl$ (**1**·HCl·2.5H_2O): C, 55.20; H, 8.18; N, 7.57. Found: C, 55.30; H, 8.07; N, 7.68.

Synthesis of Compound 8. A solution of compound **1** (107 mg, 0.35 mmol) in dioxane (20 mL) was heated to 60 °C. To this solution was added SeO_2 (78 mg, 0.7 mmol). The temperature was then increased to 80 °C. After 2.5 h, the mixture was cooled to ambient temperature. The precipitate was filtered off. The solvents were evaporated to give the crude product, which was purified by flash chromatography (silica gel, petroleum ether/0−30% ethyl acetate) to give the desired products as a yellow solid (60 mg, 57%). TLC: R_f = 0.56 (silica, 1:1 petroleum ether/ethyl acetate). Mp: 194−195 °C. ^{1}H NMR (400 MHz, $CDCl_3$, ppm): δ 10.14 (s, 1H), 7.31 (s, 1H), 6.79 (d, J = 1.76 Hz, 1H), 6.68 (d, J = 1.64 Hz, 1H), 4.12 (s, 3H), 4.02 (d, J = 6.48 Hz, 2H), 3.16 (s, 6H), 2.28 (m, 1H), 1.13 (d, J = 6.68 Hz, 6H). ^{13}C NMR (100 MHz, $CDCl_3$, ppm): δ 194.1, 160.2, 156.8, 150.6, 148.9, 134.7, 126.1, 98.1, 97.3, 91.6, 74.9, 56.2, 40.6, 28.2, 19.4. FTIR (KBr, cm^{-1}): 2967, 2917, 2807, 1618, 1600, 1499, 1471, 1438, 1415, 1379, 1309, 1260, 1243, 1211, 1158, 1124, 1068, 1000, 887, 822, 782, 723, 634, 588, 430. MS (ESI): m/z 303.2 [M + H$^+$], 325.2 [M + Na$^+$]. ESI-HRMS. Calcd for [M + H$^+$] $C_{17}H_{23}N_2O_3$: m/z 303.1709. Found: m/z 303.1700. Calcd for [M + Na$^+$] $C_{17}H_{22}N_2NaO_3$: m/z 325.1528. Found: m/z 325.1519.

Synthesis of DQCd1. To a solution of compound **8** (150 mg, 0.5 mmol) and DPA (0.1 g, 0.5 mmol) in 1,2-dichloroethane (10 mL) was added $NaBH(OAc)_3$ (0.13 g, 0.6 mmol) in portions. The resulting solution was stirred at room temperature overnight. Then the solvents were evaporated, and the solid was diluted with ethyl acetate, washed with water and brine, and dried over Na_2SO_4. The solvents were evaporated to give the crude product, which was purified by flash chromatography (silica gel, CH_2Cl_2/0−5% methanol) to give the desired products as a yellow solid (0.223 mg, 90%). TLC: R_f = 0.40 (silica, 15:1 CH_2Cl_2/MeOH). Mp: 101−102 °C. ^{1}H NMR (400 MHz, $CDCl_3$, ppm): δ 8.54 (d, J = 4.6 Hz, 2H), 7.65−7.57 (m, 4H), 7.28 (s, 1H), 7.13 (t, J = 5.72 Hz, 2H), 6.79 (d, J = 2.08 Hz, 1H), 6.66 (d, J = 1.4 Hz, 1H), 4.05−4.03 (m, 5H), 3.97 (d, J = 6.4 Hz, 2H), 3.93 (s, 4H), 3.05 (s, 6H), 2.26 (m, 1H), 1.13 (d, J = 6.68 Hz, 6H). ^{13}C NMR (100 MHz, $CDCl_3$, ppm): δ 160.9, 159.6, 156.3, 155.4, 149.2, 148.4, 136.4, 123.2, 122.8, 122.0, 100.8, 99.0, 92.5, 74.6, 61.1, 60.2, 56.0, 41.1, 28.2, 19.5. FTIR (KBr, cm^{-1}): 3051, 3011, 2959, 2929, 2872, 2815, 1621, 1589, 1503, 1469, 1435, 1360, 1258, 1218, 1176, 1144, 1087, 1047, 1024, 980, 880, 820, 765, 635. MS (ESI): m/z 486.4 [M + H$^+$], 508.3 [M + Na$^+$]. ESI-HRMS. Calcd for [M + H$^+$] $C_{29}H_{36}N_5O_2$: m/z 486.2869. Found: m/z 486.2865. Anal. Calcd for $C_{29}H_{36}N_5O_{2.5}$ (**DQCd1**·0.5H_2O): C, 70.42; H, 7.34; N, 14.16. Found: C, 70.41; H, 7.38; N, 14.04.

Synthesis of Cd-DQCd1. **DQCd1** (8 mg, 0.016 mmol) was dissolved in 1 mL of methanol. To this solution was added $CdCl_2$·2.5 H_2O (4 mg, 0.018 mmol) at room temperature. The mixture was shaken for 5 min and placed in a glass tube. Ethyl ether was then added carefully to the tube. After several days, colorless crystals of the Cd complex appeared and were ready for X-ray diffraction. ^{1}H NMR (400 MHz, DMSO-d_6, ppm): δ 9.0 (d, J = 4.6 Hz, 2H), 7.95 (t, J = 7.12 Hz, 2H), 7.54 (t, J = 6.24 Hz, 2H), 7.48 (d, J = 7.8 Hz, 2H), 7.0 (s, 1H), 6.93 (s, 1H), 6.65 (s, 1H), 4.28 (s, 3H), 4.08−4.02 (m, 8H), 3.04 (s, 6H), 2.19 (m, 1H), 1.06 (d, J = 6.6 Hz, 6H). FTIR (KBr, cm^{-1}): 2961, 2930, 2875, 2806, 1623, 1591, 1510, 1466, 1439, 1417, 1387, 1349, 1267, 1223, 1151, 1125, 1075, 1016, 997, 907, 827, 768, 640, 544, 483. ESI-HRMS. Calcd for [**DQCd1** + Cl$^-$ + Cd^{2+}] $C_{29}H_{35}CdClN_5O_2$: m/z 634.1513. Found: m/z 634.1501.

Synthesis of Zn-DQCd1. **DQCd1** (8 mg, 0.016 mmol) was dissolved in 1 mL of methanol. To this solution was added an aqueous $Zn(NO_3)_2$ solution (90 μL, 0.2 M) at room temperature. The mixture was shaken for 5 min and placed in a glass tube. Ethyl ether was then added carefully to the tube. After several days, colorless crystals of the zinc complex appeared and were ready for X-ray diffraction. ^{1}H NMR (400 MHz, DMSO-d_6, ppm): δ 8.59 (d, J = 5.16 Hz, 2H), 8.1 (t, J = 7.6 Hz, 2H), 7.66 (d, J = 7.88 Hz, 2H), 7.61 (t, J = 6.32 Hz, 2H), 7.0 (s, 1H), 6.93 (s, 1H), 6.59 (s, 1H), 4.52 (q, J = 16.44 Hz, 4H), 4.30 (s, 2H), 4.27 (s, 3H), 4.01 (d, J = 6.36 Hz, 2H), 3.06 (s, 6H), 2.15 (m, 1H), 1.02 (d, J = 6.6 Hz, 6H). FTIR (KBr, cm^{-1}): 3486, 2962, 2930, 1614, 1590, 1512, 1469, 1385, 1303, 1224, 1153, 1076, 1023, 994, 912, 803, 769, 648, 501. ESI-HRMS. Calcd for [**DQCd1** + NO_3^- + Zn^{2+}] $C_{29}H_{35}N_6O_5Zn$: m/z 611.1960. Found: m/z 611.1957.

Quantum Yield Measurements. The quantum yield for fluorescence was obtained by a comparison of the integrated area of the corrected emission spectrum of the samples with that of a solution of quinine sulfate in 0.1 N H_2SO_4 (Φ = 0.54).[29] The concentration of the reference was adjusted to match the absorbance of the test sample. Quantum yields of the metal-free ligands were measured in a HEPES buffer (10 mM HEPES, 0.1 M NaCl, pH = 7.4) containing 25 μM ethylenediaminetetraacetic acid (EDTA). Quantum yields of metal-bound ligands were measured in the HEPES buffer containing 10 μM $Cd(ClO_4)_2$ or $Zn(ClO_4)_2$. The concentration of the reference was adjusted to match the absorbance of the test sample at the wavelength of excitation. Emission for each compound was integrated from 400 to 650 nm with excitation at 360 nm. The quantum yields were calculated with the expression in eq 1.

$$\Phi_{sample} = \Phi_{standard}\frac{\int \text{emission}_{sample}}{\int \text{emission}_{standard}} \quad (1)$$

Determination of Protonation Constants. The apparent pK_a was measured by plotting the emission intensity and UV−vis absorption at selected wavelengths against the pH recorded in the range from ~2 to ~11. A solution of **1** and **DQCd1** containing 10 mM HEPES and 0.1 M NaCl was acidified by adding HCl (6 N), and the UV−vis (20 μM) and fluorescence spectra (10 μM) were recorded. Aliquots of 6, 3, 1, 0.5, and 0.1 N NaOH were added to achieve the appropriate pH changes (ΔpH = 0.3−0.5), and the UV−vis and fluorescence spectra were recorded after each addition. The overall volume change for each experiment did not exceed ~2%. Throughout the titration, the temperature was maintained at 25 ± 0.5 °C by circulating constant-temperature water through the water jacket of the titration cell. The resulting absorption (A) or normalized fluorescence emission intensity (F) was plotted as a function of the pH and fitted to the expression in eq 2[30] to calculate the pK_a values. ΔY_1 and ΔY_2 are the maximum absorption (A) or fluorescence emission intensity (F) changes associated with the corresponding pK_a values.

$$\Delta Y = \frac{\Delta Y_1}{1 + 10^{pH - pK_{a1}}} + \frac{\Delta Y_2}{1 + 10^{pH - pK_{a2}}} \quad (2)$$

Determination of Dissociation Constants. Fluorescence intensity ratio values of 10 μM **DQCd1** as a function of the free metal-ion concentration were measured in a HEPES buffer solution. Free Cd^{2+} concentrations were obtained by using a 1 mM EDTA, 5 mM

$Mg(NO_3)_2$, and 0.05−0.9 mM $Cd(ClO_4)_2$ buffer system. Free Zn^{2+} concentrations were obtained by using a 2 mM NTA and 0.2−1.9 mM $Zn(ClO_4)_2$ buffer system (see the Supporting Information). The solutions were allowed to equilibrate at 25 ± 0.5 °C for 5 min after each addition. The ratio value ($F_{495\ nm}/F_{558\ nm}$) was plotted and fitted to eqs 3 and 4 as described.[31]

$$R(\lambda^1_{em}/\lambda^2_{em}) = \frac{[M^{2+}]_{free}R_{max} + K_d\xi R_{min}}{K_d\xi + [M^{2+}]_{free}} \quad (3)$$

$$\xi = \frac{F_{min}(\lambda^2_{em})}{F_{max}(\lambda^2_{em})} \quad (4)$$

Metal-Ion Selectivity. The fluorescence spectra of 2 mL aliquots of 10 μM **DQCd1** were acquired in a HEPES buffer solution after the addition of an aliquot of metal stock solutions [the final metal's concentrations are 1.0 mM for KNO_3, $Mg(NO_3)_2$, or $Ca(NO_3)_2$ and 10 μM for $MnCl_2$, $FeSO_4$ (newly prepared), $Co(NO_3)_2$, $NiSO_4$, $Cu(NO_3)_2$, $Zn(ClO_4)_2$, $HgCl_2$, or $Pb(NO_3)_2$]. After acquisition, an aliquot of $Cd(ClO_4)_2$ (10 μM) was further titrated into the relevant solutions, and the fluorescence values of competing samples were measured again. Excitation was provided at 405 nm, and the emission intensity ratio R was calculated as $F_{495\ nm}/F_{558\ nm}$. The same experimental procedures were repeated in the presence of 50 and 500 μM NTA, respectively. The effects of counteranions such as NO_3^-, SO_4^{2-}, CO_3^{2-}, SO_3^{2-}, ClO_4^-, and AcO^- on the emission of **DQCd1** were also examined, and no interference was observed (Figure S11 in the Supporting Information).

X-ray Crystallographic Analysis. Measurements were done at 113.2 K on a Rigaku RAXIS-RAPID imaging-plate diffractometer equipped with a CCD detector using Mo Kα monochromatized radiation (λ = 0.710 73 Å). Cell refinement and data reduction were accomplished by the RAPID Auto program. The structure was then solved with direct methods and refined using *SHELXL-97* software package.[32] All non-hydrogen atoms were refined anisotropically. The hydrogen atoms were located in the calculated positions and were refined as constrained to bonding atoms. Relevant crystallographic information is summarized in Table S4 in the Supporting Information, and 50% thermal ellipsoid plots are shown in Figure 6. CCDC 791755 and 791756.

Cell Culture. NIH 3T3 cells were cultured in Dulbecco's modified Eagle's medium (DMEM; Gibco) supplemented with 10% fetal calf serum (FCS; Gibco) and 100 μg/mL penicillin/streptomycin (Hyclone) at 37 °C in a 5:95 CO_2/air incubator. The cells were cultured 3 days before dye loading onto 35-mm-diameter glass-bottomed coverslips. Then the cells were washed with PBS, bathed in PBS containing 10 μM probe **DQCd1** for 30 min at 37 °C, washed with PBS three times to remove the excess sensor, and bathed in PBS (2 mL) before imaging.

HEK293 cells were cultured in DMEM supplemented with 10% FCS and 100 μg/mL penicillin/streptomycin at 37 °C in a 5:95 CO_2/air incubator. The cells were cultured 3 days before dye loading onto 35-mm-diameter glass-bottomed coverslips. Then the cells were washed with PBS, bathed in serum-free DMEM containing 10 μM probe **DQCd1** for 30 min at 37 °C, washed with PBS three times to remove the excess sensor, and bathed in PBS (2 mL) before imaging.

Fluorescence Imaging. Confocal fluorescence imaging experiments were performed with an Olympus FV-1000 laser-scanning microscopy system, based on an IX81 inverted microscope (Olympus, Japan). The microscope was equipped with multiple visible laser lines (405, 458, 488, 515, 543, and 635 nm; continuous wave) and an UPLSAPO 60×/NA 1.42 objective. Images were collected and processed with Olympus FV10-ASW version 0107A-1 software.

For investigation of the intracellular distribution of **DQCd1**, 5 μM **DQCd1** and 1 μM Lysotracker Red DND-99 in the culture media containing 0.2% (v/v) DMSO were added to the cells, and the cells were incubated for 30 min at 37 °C. After washing with PBS (5 mL × 3) to remove the excess sensor, the cells were then filled with 2 mL of PBS for fluorescence imaging. The cells were imaged with a FV1000 confocal laser-scanning microscope equipped with the appropriate excitation and emission filters for **DQCd1** (λ_{ex} = 405 nm; λ_{em} = 425−475 nm) and Lysotracker Red (λ_{ex} = 543 nm; λ_{em} = 555−655 nm).

For ratiometric imaging of intracellular Cd^{2+}, 10 μM **DQCd1** in the culture media containing 0.2% (v/v) DMSO was added to the cells, and the cells were incubated for 30 min at 37 °C. After washing with PBS (5 mL × 3) to remove the excess sensor, the cells were treated with 30 μM $CdCl_2$ in PBS for 5−60 min. Fluorescence at two emission channels of 430−490 and 530−590 nm was measured at room temperature by excitation at 405 nm. The ratio images of $F_{430-490\ nm}/F_{530-590\ nm}$ were obtained on a pixel-by-pixel basis using FV10-ASW version 0107A-1 software. Subsequent treatment with TPEN (50 μM in the media) was performed directly on the microscope stage. Images were then collected and processed again with the Olympus FV1000 system.

■ ASSOCIATED CONTENT

Supporting Information. Synthetic procedures, characterization, and additional fluorescence and UV−vis absorption spectra of **1**, **1**·HCl, and **DQCd1**, ^1H and ^{13}C NMR, $^1H-^1H$ COSY, and HMBC spectra, and X-ray crystallographic data of **Zn-DQCd1** and **Cd-DQCd1** in CIF format. This material is available free of charge via the Internet at http://pubs.acs.org.

■ AUTHOR INFORMATION

Corresponding Author
*E-mail: hjiang@iccas.ac.cn.

■ ACKNOWLEDGMENT

We thank the Chinese Academy of Sciences "Hundred Talents Program", the National Natural Science Foundation of China (Grant 90813002), the National Basic Research Program of China (No. 2011CB935800), and the Key Laboratory of Pesticide & Chemical Biology, Ministry of Education, Central China Normal University for financial support.

■ REFERENCES

(1) (a) Friberg, L.; Elinder, C. G.; Kjellström, T. *Cadmium*; World Health Organization: Geneva, Switzerland, 1992. (b) Waalkes, M. P.; Coogan, T. P.; Barter, R. A. *Crit. Rev. Toxicol.* **1992**, *22*, 175–201. (c) Jin, T.; Lu, J.; Nordberg, M. *Neurotoxicology* **1998**, *19*, 529–535. (d) Waalkes, M. P. *J. Inorg. Biochem.* **2000**, *79*, 241–244. (e) Nordberg, M.; Nordberg, G. F. In *Heavy Metals in the Environment*; Sarkar, B., Ed.; Marcel Dekker: New York, 2002; pp 231−270. (f) Satarug, S.; Moore, M. R. *Environ. Health Perspect.* **2004**, *112*, 1099–1103.

(2) (a) United States Environmental Protectioin Agency, http://water.epa.gov/drink. (b) World Health Organization, Avenue Appia 20, 1211 Geneva 27, Swizerland, http://www.who.int/ water_sanitation_health/dwq/chemicals/cadmium/en/.

(3) (a) Petering, H. G.; Johnson, M. A.; Stemmer, K. L. *Arch. Environ. Health* **1971**, *23*, 93–101. (b) Pond, W. G.; Walker, E. F., Jr. *Proc. Soc. Exp. Biol. Med.* **1975**, *148*, 665–668. (c) Nordberg, G. F.; Fowler, B. A.; Friberg, L.; Jernelöv, A.; Nelson, N.; Piscator, M.; Sandstead, H.; Vostal, J.; Vouk, V. B. *Environ. Health Perspect.* **1978**, *25*, 3–41. (d) Benters, J.; Flögel, U.; Schäfer, T.; Leibfritz, D.; Hechtenberg, S.; Beyerwmann, D. *Biochem. J.* **1997**, *322*, 793–799. (e) Smirnova,

I. V.; Bittel, D. C.; Ravindra, R.; Jiang, H.; Andrews, G. K. *J. Biol. Chem.* **2000**, *275*, 9377–9384.

(4) (a) Smith, J. B.; Dwyer, S. D.; Smith, L. *J. Biol. Chem.* **1989**, *264*, 7115–7118. (b) Brown, E. M.; Pollak, M.; Hebert, S. C. *Annu. Rev. Med.* **1998**, *49*, 15–29. (c) Yamagami, K.; Nishimura, S.; Sorimachi, M. *Brain Res.* **1998**, *798*, 316–319. (d) Reddy, R. S.; Jinna, R. R.; Uzodinma, J. E.; Desaiah, D. *Bull. Environ. Contam. Toxicol.* **1988**, *41*, 324–328. (e) Lacroix, A.; Hontela, A. *Comp. Biochem. Phys. C* **2006**, *144*, 141–147.

(5) (a) Antonio, M. T.; Corredor, L.; Leret, M. L. *Toxicol. Lett.* **2003**, *143*, 331–340. (b) López, E.; Arce, C.; Oset-Gasque, M. J.; Cañadas, S.; González., M. P. *Free Radical Biol. Med.* **2006**, *40*, 940–951.

(6) (a) Waisberg, M.; Joseph, P.; Hale, B.; Beyersmann, D. *Toxicology* **2003**, *192*, 95–117. (b) Bridges, C. C.; Zalups, R. K. *Toxicol. Appl. Pharmacol.* **2005**, *204*, 274–308.

(7) McRae, R.; Bagchi, P.; Sumalekshmy, S.; Fahrni, C. J. *Chem. Rev.* **2009**, *109*, 4780–4827.

(8) (a) Choi, M.; Kim, M.; Lee, K. D.; Han, K.-N.; Yoon, I.-A.; Chung, H.-J.; Yoon, J. *Org. Lett.* **2001**, *3*, 3455–3457. (b) Prodi, L.; Montalti, M.; Zaccheroni, N.; Bradshaw, J. S.; Izatt, R. M.; Savage, P. B. *Tetrahedron Lett.* **2001**, *42*, 2941–2944. (c) Gunnlaugsson, T.; Lee, T. C.; Parkesh, R. *Org. Lett.* **2003**, *5*, 4065–4068. (d) Bronson, R. T.; Michaelis, D. J.; Lamb, R. D.; Husseini, G. A.; Farnsworth, P. B.; Linford, M. R.; Izatt, R. M.; Bradshaw, J. S.; Savage, P. B. *Org. Lett.* **2005**, *7*, 1105–1108. (e) Lu, C.; Xu, Z.; Cui, J.; Zhang, R.; Qian, X. *J. Org. Chem.* **2007**, *72*, 3554–3557. (f) Tang, X.; Peng, X.; Dou, W.; Mao, J.; Zheng, J.; Qin, W.; Liu, W.; Chang, J.; Yao, X. *Org. Lett.* **2008**, *10*, 3653–3656. (g) Soibinet, M.; Souchon, V.; Leray, I.; Valeur, B. *J. Fluoresc.* **2008**, *18*, 1077–1082. (h) Cockrell, G. M.; Zhang, G.; VanDerveer, D. G.; Thummel, R. P.; Hancock, R. D. *J. Am. Chem. Soc.* **2008**, *130*, 1420–1430. (i) Zhou, Y.; Xiao, Y.; Qian, X. *Tetrahedron Lett.* **2008**, *49*, 3380–3384. (j) Zhang, Y.; Chen, Y.; Li, Z.; Li, N.; Liu, Y. *Bioorg. Med. Chem.* **2010**, *18*, 1415–1420.

(9) (a) Liu, W.; Xu, L.; Sheng, R.; Wang, P.; Li, H.; Wu, S. *Org. Lett.* **2007**, *9*, 3829–3832. (b) Cheng, T.; Xu, Y.; Zhang, S.; Zhu, W.; Qian, X.; Duan., L. *J. Am. Chem. Soc.* **2008**, *130*, 16160–16161. (c) Mameli, M.; Aragoni, M. C.; Arca, M.; Caltagirone, C.; Demartin, F.; Farruggia, G.; Filippo, G. D.; Devillanova, F. A.; Garau, A.; Isaia, F.; Lippolis, V.; Murgia, S.; Prodi, L.; Pintus, A.; Zaccheroni, N. *Chem.—Eur. J.* **2010**, *16*, 919–930. (d) Yang, Y.; Cheng, T.; Zhu, W.; Xu, Y.; Qian, X. *Org. Lett.* **2011**, *13*, 264–267.

(10) (a) Grynkiewicz, G.; Poenie, M.; Tsien, R. Y. *J. Biol. Chem.* **1985**, *260*, 3440–3450. (b) Xiong, L.; Zhao, Q.; Chen, H.; Wu, Y.; Dong, Z.; Zhou, Z.; Li, F. *Inorg. Chem.* **2010**, *49*, 6402–6408. (c) Zhao, Q.; Li, F.; Huang, C. *Chem. Soc. Rev.* **2010**, *39*, 3007–3030. (d) Zhao, Q.; Huang, C.; Li, F. *Chem. Soc. Rev.* **2011**, 10.1039/C0CS00114G.

(11) (a) Peng, X.; Du, J.; Fan, J.; Wang, J.; Wu, Y.; Zhao, J.; Sun, S.; Xu, T. *J. Am. Chem. Soc.* **2007**, *129*, 1500–1501. (b) Taki, M.; Desaki, M.; Ojida, A.; Iyoshi, S.; Hirayama, T.; Hamachi, I.; Yamamoto, Y. *J. Am. Chem. Soc.* **2008**, *130*, 12564–12565. (c) Liu, Z.; Zhang, C.; He, W.; Yang, Z.; Gao, X.; Guo, Z. *Chem. Commun.* **2010**, *46*, 6138–6140.

(12) (a) Tucker, G. F.; Irvin, J. L. *J. Am. Chem. Soc.* **1951**, *73*, 1923–1929. (b) Albert, A.; Phillips, J. N. *J. Chem. Soc.* **1956**, *264*, 1294–1304. (c) Fischer, A.; Galloway, W. J.; Vaughan, J. *J. Chem. Soc.* **1964**, 3591–3596. (d) Chou, P.; Wei, C. J. *Phys. Chem.* **1996**, *100*, 17059–17066.

(13) Schulman, S. G.; Abate, K.; Kovi, P. J.; Capomacchia, A. C.; Jackman, D. *Anal. Chim. Acta* **1973**, *65*, 59–67.

(14) Since it was the first introduced into fluorescein in 1996, DPA has been widely used to construct Zn^{2+} sensors. Many reviews are available up to now. For select examples, see: (a) Kimura, E.; Aoki, S. *Biometals* **2001**, *14*, 191–204. (b) Kikuchi, K.; Komatsu, K.; Nagano, T. *Curr. Opin. Chem. Biol.* **2004**, *8*, 182–191. (c) Jiang, P.; Guo, Z. *Coord. Chem. Rev.* **2004**, *248*, 205–229. (d) Lim, N. C.; Freake, H. C.; Brückner, C. *Chem.—Eur. J.* **2005**, *11*, 38–49. (e) Dai, Z.; Canary, J. W. *New J. Chem.* **2007**, *31*, 1708–1718. (f) Carol, P.; Sreejith, P.; Ajayaghosh, A. *Chem. Asian J.* **2007**, *2*, 338–348. (g) Que, E. L.; Domaille, D. W.; Chang, C. J. *Chem. Rev.* **2008**, *108*, 1517–1549. (h) Domaille, D. W.; Que, E. L.; Chang, C. J. *Nat. Chem. Biol.* **2008**, *4*, 168–175. (i) Nolan, E. M.; Lippard, S. J. *Acc. Chem. Res.* **2009**, *42*, 193–203. (j) Tomat, E.; Lippard, S. J. *Curr. Opin. Chem. Biol.* **2010**, *14*, 225–230. (k) Xu, Z.; Yoon, J.; Spring, D. R. *Chem. Soc. Rev.* **2010**, *39*, 1996–2006.

(15) (a) Xue, L.; Liu, C.; Jiang, H. *Org. Lett.* **2009**, *11*, 1655–1658. (b) Xue, L.; Liu, Q.; Jiang, H. *Org. Lett.* **2009**, *11*, 3454–3457.

(16) Giumanini, A. G.; Chiavari, G.; Musiani, M. M.; Rossi, P. *Synthesis* **1980**, *9*, 743–746.

(17) (a) Nolan, E. M.; Burdette, S. C.; Harvey, J. H.; Hilderbrand, S. A.; Lippard, S. J. *Inorg. Chem.* **2004**, *43*, 2624–2635. (b) Goldsmith, C. R.; Lippard, S. J. *Inorg. Chem.* **2006**, *45*, 6474–6478. (c) Wong, B. A.; Friedle, S.; Lippard, S. J. *J. Am. Chem. Soc.* **2009**, *131*, 7142–7152.

(18) Christensen, J. J.; Izatt, R. M.; Wrathall, D. P.; Hansen, L. D. *J. Chem. Soc. A* **1969**, 1212–1223.

(19) Lin, X.; Wang, H.; Wang, X.; Jiang, H. *Inorg. Chem.* **2008**, *47*, 4310–4318.

(20) Martell, A. E.; Smith, R. M. *Critical Stability Constants. Amino Acids*; Plenum Press: New York, 1974; Vol. 1.

(21) Friberg, L., Nordberg, G. F., Vouk, V. B., Eds. *Handbook of the toxicology of metals*; Elsevier: Amsterdam, The Netherlands, 1986; pp 130−184; Vol. II.

(22) Kerfoot, W. B.; Jacobs, S. A. *Environ. Sci. Technol.* **1976**, *10*, 662–667.

(23) von Zglinicki, T.; Edwall, C.; Ostlund, E.; Lind, B.; Nordberg, M.; Ringertz, N. R.; Wroblewski, J. *J. Cell Sci.* **1992**, *103*, 1073–1081.

(24) Mart, L.; Nürnberg, H. W.; Valenta, P. *Fresenius' Z. Anal. Chem.* **1980**, *300*, 350–362.

(25) Chan, M.; Huang, S. *Talanta* **2000**, *51*, 373–380.

(26) The cadmium salt was added as a solid of cadmium chloride.

(27) The zinc salt was added as an aqueous solution (0.2 M) of zinc nitrate.

(28) Williams, N. J.; Gan, W.; Reibenspies, J. H.; Hancock, R. D. *Inorg. Chem.* **2009**, *48*, 1407–1415.

(29) Demas, J. N.; Grosby, G. A. *J. Phy. Chem.* **1971**, *75*, 991–1024.

(30) Burdette, S. C.; Walkup, G. K.; Spingler, B.; Tsien, R. Y.; Lippard, S. J. *J. Am. Chem. Soc.* **2001**, *123*, 7831–7841.

(31) Cielen, E.; Stobiecka, E.; Tahri, A.; Hoornaert, G. J.; De Schryver, F. C.; Gallay, J.; Vincent, M.; Boens, N. *J. Chem. Soc., Perkin Trans. 2* **2002**, *2*, 1197–1206.

(32) (a) Sheldrick, G. M *SHELXS97, Program for Crystal Structure Determination*; University of Göttingen: Göttingen, Germany, 1997. (b) Sheldrick, G. M. *SHELXL97, Program for Crystal Structure Refinement*; University of Göttingen: Göttingen, Germany, 1997. (c) Sheldrick, G. M. *Acta Crystallogr.* **2008**, *A64*, 112–122.